Available online at www.sciencedirect.com
ScienceDirect
Solid State Communications 143 (2007) 171–175
solid state communications
www.elsevier.com/locate/ssc

Anisotropic pinning in Nb thin films with triangular pinning arrays

R. Cao[a], T.C. Wu[b], P.C. Kang[a], J.C. Wu[a], T.J. Yang[b], Lance Horng[a,*]

[a] Department of Physics, National Changhua University of Education, Changhua 500, Taiwan
[b] Department of Electrophysics, National Chiao Tung University, Hsinchu 300, Taiwan

Received 20 March 2007; accepted 24 April 2007 by F. Peeters
Available online 3 May 2007

Abstract

A superconducting thin film with regular triangular arrays has been fabricated to explore the anisotropic vortex pinning behavior. We found that the critical currents for these films depend strongly on the current directions. Some interesting temperature-dependent phenomena are observed and discussed. We also made molecular dynamic simulations to study the dynamics of the vortex motion. The simulation results confirm the anisotropic features we found in the experiments.

PACS: 74.25.Qt; 74.25.Sv; 74.25.Fy; 74.78.Db

Keywords: A. Superconductors; A. Thin films; D. Vortex

1. Introduction

Vortex dynamics in the mixed state in type II superconductors is strongly influenced by the presence of defects, which act as pinning centers. During the past decade, artificial periodic pinning array has attracted a lot of research interest [1–7]. Due to the symmetry of the periodic pinning array, they are good candidates for the study of the behavior of vortex pinning. One common phenomenon for all kinds of periodic pinning arrays is the so-called matching effect, i.e., the pinning is enhanced at magnetic fields where vortex density matches the density of pinning sites. The early interests and explorations were mainly focused on square arrays of circular pinning centers. Recently, anisotropic vortex pinning has been explored for a square array of rectangular antidots [7]. Currents are applied in two perpendicular current directions in that research, and the critical current is found to be higher when the current is applied parallel to the long side of the antidots.

Triangular arrays are another kind of good candidate for the study of anisotropic vortex pinning. In this research, currents are applied in two perpendicular current directions along the triangular arrays of circle pinning sites to investigate the anisotropic properties of pinning effect. The critical current (I_c) curves reveal strong anisotropic properties. The anisotropy does not come from anisotropic pinning of individual antidots as in [7], because antidots are circular here. In this research, the anisotropy originates from the anisotropic collective pinning potential.

2. Experiment

2.1. Experimental details

In this work, electron beam lithography and reaction dry etching techniques were used to prepare a triangular lattice of defects acting as pinning centers on Si_3N_4 wafer. Briefly, e-beam lithography was used to define the designed structure into an electron sensitive resist (PMMA) which is coated on top of Si_3N_4 substrate. After the development process, the sample was etched in a chamber with plasma of oxygen gas and CF_4 gas whose ratio is 1:8. Following this, a 100-nm-thick superconducting Nb film was grown on top of the fabricated submicron holes by DC magnetron sputtering. This process is similar to our previous reports [8,9]. Fig. 1(a) is an atomic force microscopy (AFM) image of the Nb film on top of the hole array after patterning. It shows that the diameter of the hole is around 300 nm and the spacing between the

* Corresponding author. Fax: +886 4 721 1153.
E-mail address: phlhorng@cc.ncue.edu.tw (L. Horng).

0038-1098/$ - see front matter © 2007 Elsevier Ltd. All rights reserved.
doi:10.1016/j.ssc.2007.04.037

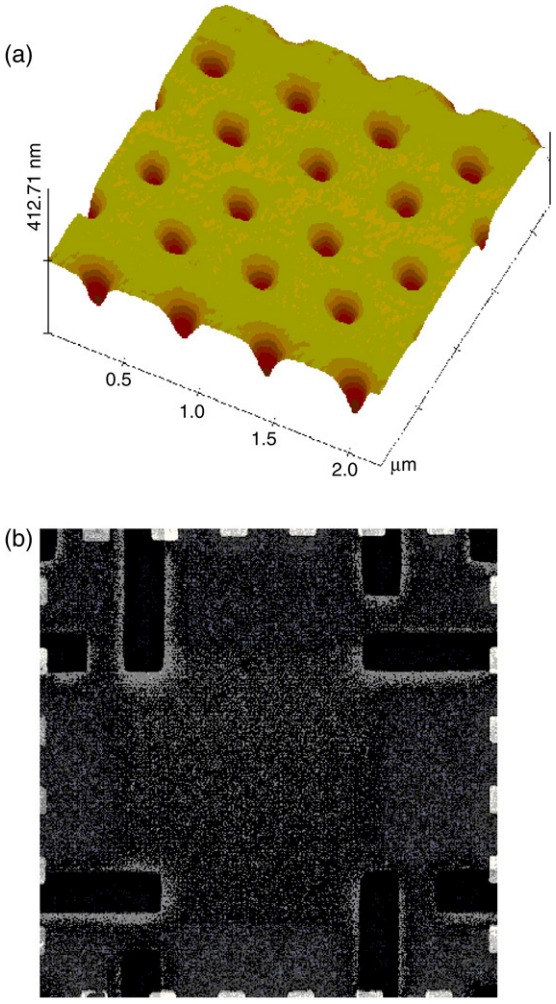

Fig. 1. (a) AFM image of the Nb film on top of the hole array after patterning. (b) SEM micrograph of the special cross-shaped bridge.

holes is around 545 nm. These length scales are comparable with the superconducting coherence length and penetration depth of Nb close to critical temperature. Magnetotransport measurements were carried out by a four-probe technique in a SQUID system with a low temperature fluctuation. The external magnetic field was applied perpendicular to the film plane and transport current. Fig. 1(b) shows a special cross-shaped bridge that can carry two perpendicular paths of driving current. The resistivity of the Nb device shows a metallic behavior as a function of temperature from room temperature to the onset of superconductivity, and the superconducting transition T_{C0} is 8.56 K at zero field.

2.2. Results and discussion

Fig. 2 shows the normalized critical current as a function of magnetic field at different temperatures along two perpendicular driving current directions; one is along the short diagonal in the rhombic unit cell of the hole array (case A) and the other is along the perpendicular direction (case B). The $I_c(H)$ curves reveal a set of maxima at equal external magnetic field interval for both cases. The interval between two consecutive maxima is 80 G, which corresponds to a vortex

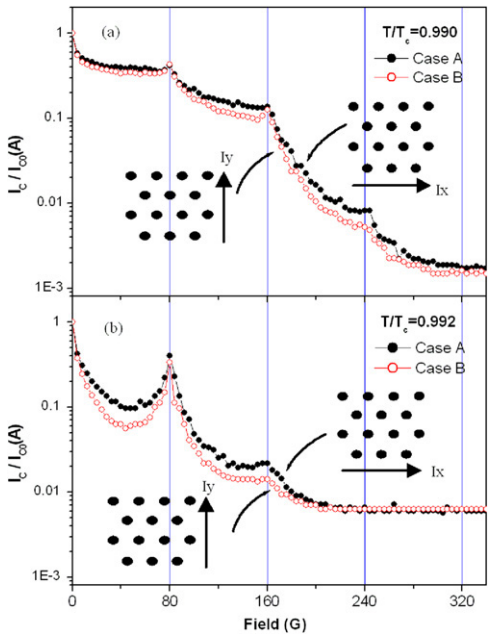

Fig. 2. Critical current as a function of the magnetic field for a Nb film with a triangular array of defects for different temperature. These curves are for case A (●) and case B (○), respectively.

density $B_1 = 1.155 \times \Phi_0/a^2$. This is in good agreement with the pinning center density of the triangular pinning array. When the applied field is not at the matching field, the vortices will form incommensurate rows or occupy interstitial sites. Thus the critical depinning force will be lower and the critical currents will be lower also.

Significant anisotropy is found in the critical current versus applied magnetic field curves for current applied in different directions, as shown in Fig. 2. The critical current for current applied parallel to a short diagonal is higher than that for current applied along the long diagonal. At the first matching field, the vortex–vortex interaction between the vortices which are pinned in the defects cancels out, and the depinning of these vortices is only determined by the pinning force, which does not depend on the driving force direction. So the critical current is the same for both cases. However, when the applied field departs from the first matching field, the critical current in case A is higher than that in case B. In those situations, the interstitial vortices are in an anisotropic pinning potential which is created by the vortices at the pinning sites and the other interstitial vortices. If there are no interstitial vortices, then the vortices in the pinning sites will form incommensurate rows and will also experience an anisotropic pinning potential.

Fig. 2 also shows the impact of temperature on the critical current curves. Fig. 2(a) is measured at $T/T_c = 0.990$ and Fig. 2(b) is measured at $T/T_c = 0.992$. When temperature is high, the penetration depths of the vortices are long and the interactions between them are strong. This is an important factor we should keep in mind when explaining the temperature related phenomenon. One obvious difference between Fig. 2(a) and (b) is that at the second matching field, critical currents are almost the same for case A and B at $T/T_c = 0.990$, but different at $T/T_c = 0.992$. This result indicates that there

are two vortices at each pinning site at $T/T_c = 0.990$, and only one vortex at each pinning site at $T/T_c = 0.992$. For lower temperature, the interaction between vortices is weaker, and the pinning site will be capable of catching two or more vortices. Thus at the second matching field, there will be no interstitial vortices and the depinning of a vortex will be mainly determined by the pinning force it experiences and its interaction with the vortex occupying the same pinning site. The critical current will be the same for both case A and case B. This should be what must have happened at $T/T_c = 0.990$. If there are interstitial vortices, they will be in an anisotropic potential landscape and will have different critical currents. This would be the case for $T/T_c = 0.992$.

The critical currents at the third matching field are different for case A and B at $T/T_c = 0.990$, this indicates that there are only two vortices captured by each pinning site. We can also see that the critical current at the second matching field is much higher than that at the third matching field, and only a little lower than that at the first matching field. It supports our argument that there are no interstitial vortices at the second matching field, because the depinning of interstitial vortices will be much easier than of vortices at the pinning sites. For $T/T_c = 0.992$, the critical current at the second matching field is much lower than that at the first matching field, this also agrees with our argument that there are interstitial vortices at the second matching field at this temperature.

3. Simulation

We have used molecular dynamic simulations to study this anisotropic phenomenon in the thin film with triangular pinning array. We obtained some meaningful results similar to our experimental results.

3.1. Model

The simulation methods we used here are similar to those in [10]. We model a 2D system with periodic boundary conditions in x- and y-directions with N_v vortices interacting with N_p pinning sites. The vortex lines are parallel to the sample edges. We define $n = N_v/N_p = B/B_\Phi$, where B_Φ is the first matching field at which the number of vortices equals the number of pinning sites. We numerically integrate the overdamped equations of motion:

$$\eta v_i = f_i = f_i^{vv} + f_i^{vp} + f_d. \quad (1)$$

Here, f_i is the total force acting on vortex i, f_i^{vv} is the force on the ith vortex due to interactions with other vortices, f_i^{vp} is the vortex pin interaction force, f_d is the driving force and η is the viscosity, which is set equal to unity in this work.

$$f_i^{vv} = \sum_{j=1}^{N_v} f_0 K_1\left(\frac{|r_i - r_j|}{\lambda}\right)\hat{r}_{ij}, \quad \text{where } f_0 = \frac{\Phi_0^2}{8\pi^2\lambda^3}. \quad (2)$$

Here, $K_1(r/\lambda)$ is a modified Bessel function and λ is the penetration depth. Since the Bessel function falls off exponentially for $r > \lambda$, a cutoff can be safely placed at $r = 6\lambda$ for computational efficiency. We take λ to be 0.6 length units. Pinning is modeled as attraction parabolic wells with

$$f_i^{vp} = -\sum_{k=1}^{N_p}(f_p/r_p)\left(r_i - r_k^{(p)}\right)H\left(r_p - \left|r_i - r_k^{(p)}\right|\right). \quad (3)$$

Here, $r_k^{(p)}$ is the location of pinning site k, f_p is the maximum pinning force, r_p is the radius of the pinning site and H is the step function. The pinning sites are regular triangular arrays in our work. We take $f_p = 0.5 f_0$. We take lateral length of the triangle to be 2 length units and r_p to be 0.5 length units.

The initial positions of the vortices are obtained using a numerical algorithm simulating the annealing process [10]. After the vortex configurations are obtained, the dynamic behavior is simulated by applying a slowly increasing and spatially uniform driving force, f_d, corresponding to a Lorentz force from an applied current. The driving force is applied in two perpendicular directions, respectively, as we have discussed in the experimental part. It should be noted that when the current is applied along the short diagonal of the rhombic unit cell, the driving force is along the long diagonal. The results for this work are for 6×6 pinning arrays. We also conducted simulations for larger systems and found similar results. The critical depinning force is defined to be the force value at which the average velocity along the driving force reaches 0.01 velocity units.

3.2. Results and discussion

First, we used parameters which only allow one pinning site to capture one vortex, and the simulation results correspond to high temperature and long penetration depth situation. The major features of our experimental results for $T/T_c = 0.992$ are reproduced here. The dynamic behaviors of the vortices are very different for case A and case B. The trajectories of the vortices for driving force just above the critical depinning force for $n = 2$ are shown in Fig. 3. The interstitial vortices are moving and the vortices at the pinning sites still persist there. For case A, the current is applied along the x-direction and the driving force is along the y-direction. It is clearly seen that the interstitial vortices are driven head-on toward vortices at the pinning sites and their movement is greatly hindered by them. The interstitial vortices for case B are driven toward the space between the pinned vortices and their movements are less impacted by the vortices at the pinning sites and much smoother. These trajectories indicate that it is easier for interstitial vortices in case B to depin and move than for case A.

The simulation results for critical currents are shown in Fig. 4. The pronounced peaks for critical currents at $n = 1$ and 2 in the experiments are also obvious in the simulation results. The critical currents for $n = 1$ are the same for both case A and case B as we have explained in the experimental part. The critical currents for $n = 2$ are different for case A and case B. Because the movement of interstitial vortices is less affected by the vortices at the pinning sites for case B, the critical current is lower for case B, as indicated by the trajectories of vortices in Fig. 3. The critical currents in simulation results also have

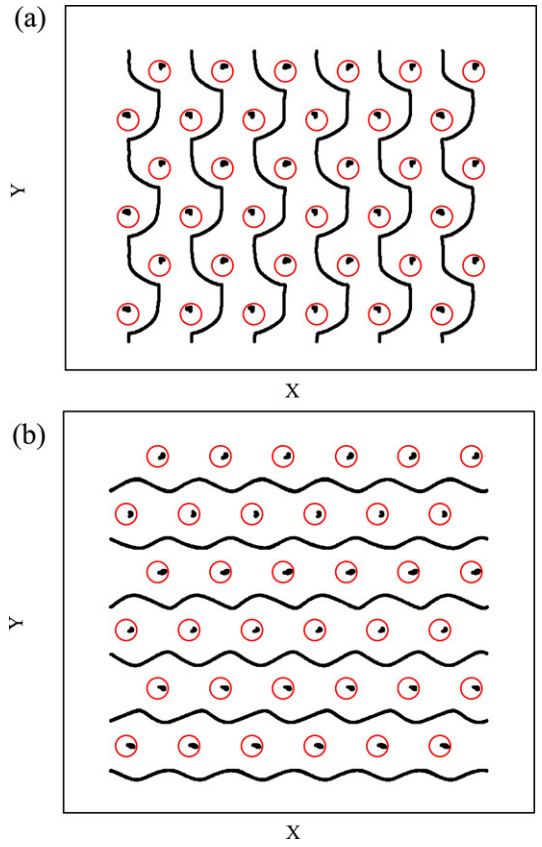

Fig. 3. The trajectories of vortices for $n = 2$ for case A (a) and case B (b) for driving force just above the critical depinning force. The open circles represent the pinning sites.

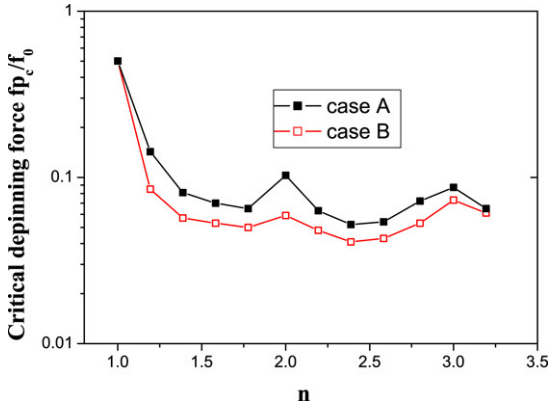

Fig. 4. Comparison of critical depinning force for case A and case B for systems with periodic triangular pinning array. Magnetic field B ranges from $0.6B_\Phi$ to $3.2B_\Phi$.

a peak at $n = 3$, which is missing in the experimental data (see Fig. 2(b)). The reason may be that the magnetic field corresponding to $n = 3$ is already higher than H_{c2} and the superconductor is in normal state in the experiments. For the fields not at the matching fields and higher than $n = 1$, the critical currents for case A is always higher than for case B. This is also in agreement with our experimental results. The depinning of interstitial vortices is similar to what happened for $n = 2$.

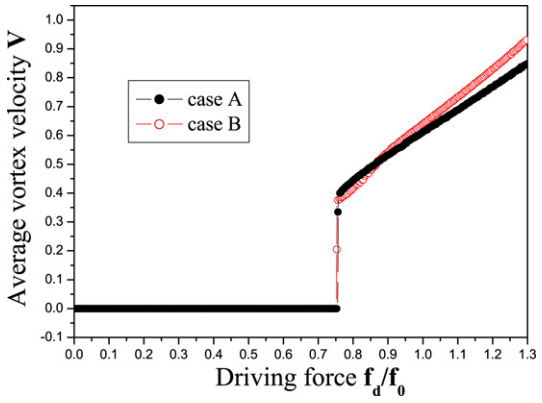

Fig. 5. Comparison of average vortex velocity versus the applied driving force for f_d in x- and y-directions for systems with triangular pinning array ($n = 2$). $F_p = 1.5f_0$ and r_p is 0.5 length units. V represents V_y for case A and V_x for case B.

We also made a few simulations with different parameters where one pinning site could be occupied by two vortices, corresponding to the situation with lower temperature. We changed F_p to be $1.5f_0$ there. The driving force vs. average velocity curves at $n = 2$ for case A and case B are shown in Fig. 5. We can see that the vortices did not depin until f_d/f_0 increases to about 0.75 and the critical depinning force is almost the same for case A and case B. This result supports our explanation of the experimental results for $T/T_c = 0.990$.

4. Conclusions

In summary, a superconducting Nb thin film with triangular arrays of pinning sites has been fabricated to investigate the vortex pinning behavior. Periodic maxima appear in the critical current curves at equal field intervals that can be associated with matching effect. The transport properties at near critical temperatures show anisotropic pinning properties related to the configuration of pinning centers. The critical current is depressed when the Lorentz force is applied along the short diagonal in the rhombic unit cell of the pinning array. The data for lower temperature indicates that two vortices may be captured by one pinning site because of the weaker vortex–vortex interaction. We also made molecular dynamic simulations to study the dynamics of vortex motion. The simulation results confirm the anisotropic phenomenon we found in the experiments. The trajectories of the vortices above the critical depinning force also indicate anisotropic potential landscape, which results in the anisotropic movement of the vortices.

Acknowledgement

This work was supported by the National Science Council of the Republic of China under Grant No. NSC 95-2112-M-018-001.

References

[1] C. Reichhardt, C.J. Olson, F. Nori, Phys. Rev. Lett. 78 (1997) 2648.
[2] O. Daldini, P. Martinoli, J.L. Olsen, G. Berner, Phys. Rev. Lett. 32 (1978) 218.

[3] A.T. Fiory, A.F. Hebard, S. Somekh, Appl. Phys. Lett. 32 (1978) 73.
[4] M. Baert, V.V. Metlushko, R. Jonckheere, V.V. Moshchalkov, Y. Bruynseraede, Phys. Rev. Lett. 74 (1995) 3269.
[5] Y. Otani, B. Pannetier, J.P. Nozieres, D. Givord, J. Magn. Magn. Mater. 126 (1993) 622.
[6] J.I. Matin, M. Velez, J. Nogues, I.K. Schuller, Phys. Rev. Lett. 79 (1997) 1929.
[7] L.V. Look, B.Y. Zhu, J. Nogues, R. Jonckheere, B.R. Zhao, Z.X. Zhao, V.V. Moshchalkov, Phys. Rev. B 66 (2002) 214511.
[8] L. Horng, J.C. Wu, P.C. Kang, P.H. Lin, T.C. Wu, Japan. J. Appl. Phys. 42 (2003) 2679.
[9] T.C. Wu, P.C. Kang, L. Horng, J.C. Wu, T.J. Yang, J. Appl. Phys. 95 (2004) 6696.
[10] C. Reichhardt, C.J. Olson, F. Nori, Phys. Rev. B 58 (1998) 6534.